Differential cross sections for electron impact excitation of the n = 2 states of helium at intermediate energies (80, 100 and 120 eV) measured across the complete angular scattering range (0180°)

R Ward, D Cubric, N Bowring, G C King, F H Read, D V Fursa, I Bray, O Zatsarinny, K Bartschat

Confidential: not for distribution. Submitted to IOP Publishing for peer review 16 December 2010

Differential cross sections for $n = 2$ states of helium at intermediate energies (80 eV, 100 eV and 120 eV) measured across the complete angular scattering range (0°-180°).

Differential cross sections for electron impact excitation of the $n = 2$ states of helium at intermediate energies (80 eV, 100 eV and 120 eV) measured across the complete angular scattering range (0°-180°).

R Ward[1,4], D Cubric[1], N Bowring[1], G C King[1], F H Read[1], D V Fursa[2], I Bray[2], O Zatsarinny[3] and K Bartschat[3].

[1] School of Physics and Astronomy, Schuster Laboratory, Manchester University, Manchester M13 9PL, UK.

[2]ARC Centre for Antimatter-Matter Studies, Curtin University of Technology, GPO Box U1987 Perth, Western Australia 6845, Australia.

[3]Department of Physics and Astronomy, Drake University, Des Moines, Iowa 50311, USA.

Abstract

Differential cross sections (DCS) for inelastic electron scattering to the $n = 2$ states in helium have been measured at incident energies of 80 eV, 100 eV and 120 eV. These DCS have been determined across the complete angular scattering range (0° to 180°) using a magnetic angle changer (MAC) with a soft-iron core. The converging close-coupling (CCC), R-matrix with pseudostates (RMPS), and B-spline R-matrix (BSR) methods have been used to calculate these DCS. Agreement between the experimental data and the predictions from these highly sophisticated theoretical methods is generally good. The remaining discrepancies mainly occur at small and large angles for the triplet states 2^3S and 2^3P, whereas excellent agreement is found between 30º-150º. The small-angle differences are likely due to contamination of the observed experimental signal from the neighbouring 2^1S and 2^1P states. The present results demonstrate the effective use of a soft-iron core magnetic angle changer for DCS measurements at intermediate energies, extending the operational energy range of such devices by a factor of approximately 25.

.

[4] Corresponding Author.

Differential cross sections for $n = 2$ states of helium at intermediate energies (80 eV, 100 eV and 120 eV) measured across the complete angular scattering range (0°-180°).

PACS numbers:

34.80.Dp Atomic excitation and ionisation

34.10.+x General theories and models of atomic and molecular collisions and interactions (including statistical theories, transition state, stochastic and trajectory models, etc.)

Differential cross sections for $n = 2$ states of helium at intermediate energies (80 eV, 100 eV and 120 eV) measured across the complete angular scattering range (0°-180°).

1. INTRODUCTION

There continues to be a great deal of interest in the study of electron impact excitation of helium, from the standpoints of both theory and experiment. On the theoretical side, helium provides a fundamental test case for the validity of the many theoretical models, especially their description of electron-electron correlations. On the experimental side, there have been numerous studies of electron impact excitation of helium. These include a number of measurements of the differential cross sections (DCS) of the $n = 2$ states of helium. A summary of these measurements up to 1992 has been given by Trajmar [1]. Further work includes that of Allan [2], Röder et al [3], Asmis and Allan [4], Cubric [5], Allan [6] and Lange et al [7]. Most recently, Hoshino et al [8] have presented DCS for the $n = 2$ states at near-ionisation threshold energies (23.5 - 35 eV). Most of the recent studies have concentrated on the low-energy regime. It is also the case that almost all of the previous experimental studies have presented data up to a maximum angular scattering range of approximately 135°. This is because higher scattering angles are inaccessible to conventional electron spectrometers as the angular range of the electron energy analyser is limited by the presence of the electron monochromator.

A number of theoretical models for DCS of specific interactions exist. Perturbative methods have existed for many years and include Coulomb Projected Born Approximation (CPB) [9]; First-Order Many-Body Theory (FOMBT) [10]; Distorted Wave Born Approximation (DWBA) [11]; Distorted-Wave Polarisation Orbital (DWPO) [12]; Multi-Channel Eikonal Approximation (MCE) [13] and Second-Order Potential Distorted-Wave (SOPDW) [14]. More recently a range of more accurate non-perturbative methods, including R-Matrix with Pseudo-States (RMPS) [15]; B-spline R-Matrix (BSR) [16] and Convergent Close-Coupling (CCC) [17], have emerged as methods that agree well with both themselves and experiment [7]. In the current work all three of these non-perturbative methods have been compared to experimental results, together with a 5-state model based on BSR and available FOMBT perturbative data

In the present work, DCS have been measured for the 2^3S, 2^1S, 2^3P and 2^1P states of helium, at the intermediate energies of 80 eV, 100 eV and 120 eV, over the complete angular scattering range 0° to 180°. The full angular scattering range has been achieved by the use of a magnetic angle changer (MAC). The intermediate energy range has been reached by the use of a MAC equipped with a soft-iron core, which allows for the device to work at high electron energies. MACs have been used previously to measure DCS in helium over the complete scattering angular range. Cubric et al [5] measured the DCS of the 2^3S, 2^1P, 2^3P and 2^1P states of helium at 30, 40 and 50 eV, while Allan [6] measured the DCS of the 2^3S state from threshold to 24 eV.

Differential cross sections for n = 2 states of helium at intermediate energies (80 eV, 100 eV and 120 eV) measured across the complete angular scattering range (0°-180°).

In addition to the present experimental measurements we have also calculated the corresponding DCS using the CCC, RMPS, and BSR methods. It is the goal of the present work to compare the experimental measurements with the results of these theories. In the following sections we briefly describe the experimental and theoretical techniques used. Measurements and calculations of the DCS, at the intermediate energies employed, are then presented and discussed in Section 4 of the paper.

2. APPARATUS AND EXPERIMENTAL PROCEDURES

Measurements of electron angular distributions in atomic and molecular physics have used various experimental configurations. A recent approach has been the adoption of the 'magnetic angle-changing technique' [18,19]. This technique produces a localized magnetic field, within the interaction region, thereby enabling controlled deflection of the electron trajectories. The first practical MAC devices, constructed at Manchester, were limited to low electron energies, below about 20 eV. This was due to the heat produced by the solenoid currents in the MAC and the need to dissipate this heat in an evacuated experimental chamber.

One solution to this problem, developed by Cubric et al [5], is to incorporate a soft-iron core within the solenoids of the MAC. This significantly increases the magnetic field in the device, and hence greatly extends the range of electron energies that can be used. The present measurements involve higher electron energies, and hence the MAC described by Cubric et al [5] has been used. It is shown schematically in figure 1. It uses two pairs of solenoids and appropriate currents flowing in opposite directions, so that the magnetic dipole moment of the MAC is zero. This, together with zero or minimal contributions from higher magnetic moments, ensures that the magnetic field has negligible effect on the operation of the electron spectrometer used in the measurements. The ferromagnetic material used for the MAC is soft iron with a magnetic permeability of approximately 1000. The magnetic hysteresis curve for soft iron is very narrow. Therefore it can be considered as a linear magnetic material, enabling currents to be applied without residual fields being generated within the angle changer. The magnetic field produced by the MAC has been measured and the results are plotted in figure 2 for a current of 1 A through the inner solenoids and a current of -0.772 A through the outer solenoids. As can be seen, the magnetic field is localized and changes its direction at a distance of about 12 mm from the central axis. Also shown in figure 2 is the magnetic field variation from a comparable MAC without an iron core (which has been multiplied by a factor of 5). The magnetic field produced by the solenoids can also be calculated, using the following equation:

$$B_\rho(z,\rho,R,I)=\frac{\mu_0 I}{4\pi}\int_0^{2\pi}\frac{\rho z\cos(\phi)}{(\rho^2+z^2+R^2-2\rho R\cos(\phi))^{3/2}}d\phi\,, \qquad (1)$$

where R is the solenoid radius and z and ρ are cylindrical polar coordinates representing respectively the axial and radial distances to the coil centre. The resulting magnetic field is due to the contributions from both solenoids. When a charged particle, with kinetic energy E, moves through a magnetic field B, it experiences a deflection proportional to B^2/E. Hence, by increasing the magnetic field by a factor of 5, using a soft-iron core, the device becomes capable of handling electron energies 25 times larger than the device without the iron core. In the present work, this has enabled the measurements at intermediate energies in the range 80 eV-120 eV. The action of the MAC for inelastic electron scattering is illustrated in figure 3. The deflection from the MAC is proportional to the beam energy. Therefore the incident beam (originating from the right side, dashed line) is deflected slightly less than the scattered beam (solid line) whose residual energy is 20 eV less. These beams are separated as they exit the MAC as can be seen at the bottom of figure 3. The full angular range of the scattered beam can be detected either by fixing the analyser and varying the MAC currents, or by fixing the currents and moving the analyser. In figure 3, using fixed MAC currents, the scattered beam can be detected across the range of 0° - 180° by rotating the electron analyser from -90° to +90° relative to the incident beam, with the electron monochromator always a significant distance from the electron energy analyser.

The MAC was used in conjunction with an electrostatic electron spectrometer, which has been described in detail previously by Bradford [20]. Briefly, it consists of an electron monochromator and an electron energy analyser, which could be rotated over the angular range from -10^o to 120^o with respect to the direction of the incident electron beam. The construction of the monochromator was based on a hemispherical selector having a mean radius of 50 mm. Two triple-aperture lenses were employed to focus the incident electron beam onto the target gas beam. A second set of two triple-aperture lenses was used to decelerate and focus scattered electrons from the target region onto the entrance aperture of a hemispherical electron analyser, again of 50 mm mean radius. Transmitted electrons were detected by a channel electron multiplier. The incident electron beam current was monitored by a rotatable Faraday cup and typically had a value of 5 nA [21]. The incident electron energy was calibrated against the position of the 2^2S resonance in helium (19.365 eV [22]) and had an uncertainty of ± 115 meV, while the energy resolution of the present measurements was typically 130 meV (full width at half maximum). The angular resolution of the measurements (full width at half maximum) was estimated to be 6° [23]. This value arose from the angular resolution of the spectrometer and the angular spread induced by the MAC [5]. The target gas beam was produced by a single capillary of internal diameter of 0.5 mm and length 10 mm, and target pressures of typically 4.5×10^{-3} Pa were employed.

For the present measurements, the MAC was operated in the following way. The electron energy analyser was held at the fixed angle of 90°, with respect to the incident electron beam direction. Appropriate solenoid currents were then used to provide deflection

angles for the scattered beam over the range ± 90°, so that a total scattering angular range of 0° to 180° was obtained. To measure a particular DCS, the yield of inelastically scattered electrons, arising from excitation of the state, was measured as a function of the scattering angle. In this procedure, care was taken to ensure that any background contributions were taken into account. These background contributions could arise from electrons scattering off residual gas in the experimental chamber or surfaces close to the interaction region. Total data accumulation times for the DCS measurements were approximately 65 hours.

Once scattering data have been obtained, there are several techniques that can be used to obtain the absolute DCS from them [24]. These include direct normalisation, which requires knowledge of the electron current, gas density etc. [25], the relative flow technique [26], and normalisation against a known cross section [27]. For the present study the most appropriate method was the use of a known DCS. The DCS of the 2^1P state was chosen as the reference, given the agreement in previous values for this state. Values for this DCS were obtained using the CCC method. Such a procedure was previously used with much success by Mercer [23] in low-energy DCS measurements for the n = 2 states in helium. By comparing the theoretical curves for the 2^1P DCS with the measured electron intensities, the transmission of the electron energy analyser, as a function of scattering angle, could be determined for each value of incident electron energy. These transmission functions were then applied to the scattering data for the remaining states (2^3P, 2^1S, 2^3S), to obtain the DCS. All measurements were obtained under identical conditions of gas flow in the interaction region.

3. CALCULATIONS OF THE DCS

We have used the CCC, RMPS, and BSR methods to calculate the DCS for the transitions and energies of interest for the present paper. Below these predictions are compared to the current experimental data, previous experimental data, and results from a few selected older theoretical approaches. The principal difference between CCC, RMPS, and BSR compared to discrete-state-only close-coupling or R-matrix approaches, such as the 5-state model including only the ground state and the four $n = 2$ states, is the coupling to both higher-lying discrete states and the ionization continuum. In principle, this coupling can be driven to convergence, and one might expect a computationally “exact” solution of the Schrödinger equation. In practice, of course, the number of states that can be included is finite, and their description is typically subject to some approximations. For example, the CCC calculations have been performed in the frozen-core model, restricting one of the target electrons always to be in the 1s orbital of He+. On the other hand, the RMPS and BSR models use a multi-configuration description of the target states, but they include less pseudostates and hence utilize a coarser discretization of the Rydberg spectrum and the ionization continuum. However, since the remaining shortcomings of these models are

essentially independent of each other, the good agreement between the CCC, RMPS, and BSR predictions shown below provides significant confidence in the reliability of these results. Finally, the FOMBT approach effectively corresponds to a 2-state model similar to the DWBA and the many other perturbative approaches used over the years. Channel coupling is neglected in these models, but an attempt is made to account for some of these effects (polarization, absorption, and sometimes exchange) indirectly by choosing what is believed to be an appropriate distortion potential for the calculation of the distorted waves

The application of the CCC method to electron-helium scattering was reviewed by Fursa and Bray [12]. Briefly, the helium target states are obtained by utilising a complete Laguerre basis. In the frozen-core approximation all configurations have the "inner" electrons described by the 1s orbital of He^+. This leads to an ionisation energy error of 0.84 eV, but has the advantage of computational simplicity. In the multi-configuration expansion we may obtain a very accurate ground state, but this comes at the expense of subsequent computational complexity in scattering calculations. It has been our experience that for processes, which are dominated by one-electron excitation, the frozen-core approximation suffices, and hence we use it here.

Using the Laguerre basis ensures that all of the target states are square-integrable. With increasing basis size the negative-energy states converge to the true discrete eigenstates, while the positive-energy states provide an increasingly dense discretization of the continuum. The states are used to expand the total wavefunction, which leads to the close-coupling equations. In the CCC method these take the form of coupled Lippmann-Schwinger equations in momentum space. They are solved utilising a partial-wave expansion, and the required excitation amplitudes are obtained. Convergence in the results of interest is checked by taking a sufficiently large basis. Presently, this is achieved by taking $N_l = 25\text{-}l$ for target space orbital angular momenta $l < 5$.

The R-Matrix with Pseudo States (RMPS) approach, developed by Bartschat et al [28,29], uses a similar idea as the CCC method described above, except that the close-coupling equations are solved in coordinate space, with a basis-function expansion for the projectile in the inner region of the R-matrix box. The advantage of using such an expansion is the computational efficiency when results for a large number of collision energies are required. This is typically the case for the low-energy near-threshold regime that is often dominated by resonances. The price to pay, on the other hand, is the fact that the number of pseudostates that can be included is generally less than what can be handled in the CCC approach. Also, the highest energy that can be treated is limited by the highest energy of the one-electron basis functions. Hence, calculations for just a few intermediate energies, as required in the present work, represent a challenge for the R-matrix approach in general. However, the rapid increase of computational resources has made such calculations possible on a more or less routine basis.

Differential cross sections for $n = 2$ states of helium at intermediate energies (80 eV, 100 eV and 120 eV) measured across the complete angular scattering range (0°-180°).

The present RMPS results were generated with the 5+36 model (5 physical states plus 36 pseudostates) described by Bartschat et al [30].The R-matrix radius was set to 27 a_0, where $a_0 = 0.529 \times 10^{-10}$ m is the Bohr radius, and 30 continuum orbitals were used per angular momentum to expand the wavefunction of the projectile in the box. We included 10 target states with 1S symmetry, 9 with ^{3}S, 8 with ^{1}P and ^{3}P each, and 3 with ^{1}D and ^{3}D each, respectively. This is a relatively small model, but we will see that it is almost sufficient for the situation of the present work.

The B-Spline R-Matrix (BSR) method, developed by Zatsarinny and Fischer [31, 32], with a computer code published by Zatsarinny [16], is an alternative to the standard R-matrix approach developed by the Belfast group [33,34]. The BSR method uses a B-spline basis to expand the target states as well as the wavefunction of the projectile inside the R-matrix box. As piecewise polynomials, the B-splines enable the Schrödinger equation to be solved in a box, which makes them very effective in forming the R-matrix basis. By diagonalizing the target hamiltonian in the B-spline basis, it is straightforward to generate a set of pseudostates, similar to what is being done in CCC and RMPS. The energy distribution of the pseudostates, however, is very different from those obtained in the Laguerre-based CCC and the Sturmian-based RMPS methods. Once again, we emphasize that agreement between the results obtained in these entirely independent computational implementations for solving the Schrödinger equation for this collision problem provides confidence in the theoretical predictions.

Specifically, the current BSR model included 126 target states, of which the lowest few (including the ground state and the $n = 2$ states) were described very well by multi-configuration expansions. A major advantage of the BSR method is the ability to used term-dependent one-electron orbitals, i.e., in the present problem the only role of the pseudostates is to approximate the coupling to the higher Rydberg states and the target continuum. In the RMPS approach, on the other hand, the pseudostates also improve – at least to some extent – the target description itself. Specifically, the 126-state BSR model used an R-matrix radius of 40 a_0, included 59 B-splines to cover this radial grid, and contained 23 bound states, 96 pseudo-states, and the 7 doubly excited autoionizing $2l2l'$ states. All target states had total orbital angular momenta $L = 0$, 1, or 2.

The 5-state model is used in the current work to investigate the effect of additional channel coupling compared to other models. Since it employs the same target description for the ground state and the $n = 2$ states, comparing the results from the 5-state and the 126-state BSR models provides an indication about the importance of the additional coupling to the higher discrete states and the ionisation continuum. Based on previous experience, one would generally expect the largest differences between the 5-state results and those from CCC, RMPS, and BSR with many pseudo-states to appear in the results for the triplet states, with some difference in 2^1S, and little in 2^1P.

Differential cross sections for n = 2 states of helium at intermediate energies (80 eV, 100 eV and 120 eV) measured across the complete angular scattering range (0°-180°).

Trajmar et al [1] have previously provided data using First-Order Many Body Theory (FOMBT) for the 2^1P state at 80 eV and 100 eV. These have been included in the current work to illustrate the comparison with this earlier modelling, which was originally developed in the 1970s [35]. One would expect the perturbative FOMBT model to do reasonably well for the optically allowed 1^1S –> 2^1P transition, since at the energies under consideration the result is mostly determined by the generalized oscillator strength, i.e., an element of the structure rather than the collision model.

4 RESULTS AND DISCUSSION

4.1 DCS results at 80 eV

Measurements of the DCS at 80 eV for the 2^1P, 2^1S, 2^3P and 2^3S states of helium are shown in figures 4 - 7. All the error bars shown on all the spectra represent a one standard deviation estimate of the uncertainty of the measured intensity. The experimental results are presented together with the results of the CCC, RMPS, and BSR calculations, the latter performed with 126 states (i.e., also in the RMPS mode) and only the lowest five physical target states. Also shown for the 2^1P state are the theoretical and experimental results of Cartwright et al [36] who compared FOMBT calculations to their experimental results. Note that each vertical scale, corresponding to the value of the cross section, is logarithmic.

The 2^1P data shows excellent agreement between previous experimental data and the current data, and between both experimental data and the BSR and CCC models across the angular range. RMPS deviates slightly from these results at very small angles below 10° and very large angles above 170°. The 5-state and FOMBT models overestimate the cross section beyond 90° and FOMBT also deviates significantly from the other results between 40° and 75°. There is a minor difference in the two experimental data sets below 10°.

The 2^1S data shows good agreement with the CCC results across the majority of angles (20° - 160°) and is consistent in the angular dependence with both BSR and RMPS over this range, where the experimental cross section is consistently slightly lower than predicted by these models. The 5-state model shows very good agreement with experiment below 20° but beyond this differs significantly from the remainder of the data. Beyond 160° the experimental cross section is lower than the theoretical results, also exhibiting a slight downward slope. The minimum in the DCS at approximately 45º is confirmed together with the shape around this minimum. The observed minimum near 45º and the large-angle dependence of the DCS also agree with previous experimental data [37,1] (not shown in the figure).

The 2^3P DCS agrees broadly with the theoretical models for the angular range between 25º and 160º. The agreement is especially good with the BSR predictions while the CCC results lie somewhat below the experimental data points, and the RMPS data vary significantly between 120° and 160°. Below about 25º the theoretical predictions deviate strongly from the experimental data, with the theoretical results showing a local maximum

near 25º and a decreasing cross section below 25º. By contrast, the experimental data increases rapidly below 25º. This discrepancy could be due to larger uncertainties in the experimental data for the 2^3P state in this angular range. The increase in uncertainty arises because the 2^3P lies close in energy to the 2^1P state (250 meV energy separation), which has a much larger signal for forward scattering. Thus, due to the finite resolution of the electron spectrometer (typically 130 meV), the 2^3P signal may have a contribution from the 2^1P state. Several calculations were performed to check the convergence utilising the frozen-core and multi-configuration models, at this and the other considered energies. No substantial variation at the forward angles was found. To simulate the possible effect, adding a 1% contribution of the 2^1P signal with the RMPS data has also been modelled. The results suggest that the experimental discrepancy at small angles is indeed likely due to a contamination from the 2^1P signal and explains the discrepancy from theory for pure exchange transitions. There is no clear evidence of the shallow maximum suggested by the RMPS model near 150º. This may be due to insufficient statistical accuracy in the data at large angles, where the signal counting rate falls rapidly. Indeed, the results between 160° and 180° agree well with RMPS and deviate somewhat from both BSR and CCC where the experimental cross section is higher, unlike the 2^1S DCS where the opposite is true.

The measured 2^3S DCS shows least agreement with the theoretical results. However, there is general agreement with respect to the overall shape of the DCS and its magnitude. The largest discrepancy between experiment and theory occurs above about 90º, where the theoretical results lie appreciably above the experimental data. Moreover the theoretical values do not reflect the drop in the DCS beyond 150º that is observed in the experiment. At very small angles (below 10°), the experimental data again are higher than the most sophisticated theoretical predictions, which show very good agreement with each other. In this case, however, it is currently unclear why such a strong contamination should have occurred. This anomaly should be investigated further and is discussed in the sub-section below for the 2^3S DCS at 100 eV. The significant dip observed in the DCS at approximately 48º is sharper in the experimental data than in the theories, but advances in theoretical modelling are progressing towards the experimental angular dependence in this angular range.

4.2 DCS results at 100 eV

The measurements of the DCS at 100 eV for the 2^3S, 2^1S, 2^3P and 2^1P states of helium are shown in figures 8 - 11. The experimental results are again presented together with the theoretical results of the CCC, RMPS, and the two BSR calculations. Also shown for the 2^1P state are the theoretical and experimental results of Cartwright et al [36] who compared FOMBT predictions to their experimental results. For the 2^3S, 2^3P, and 2^1S states the experimental data of Trajmar et al [1] are also presented.

The 2^1P data show excellent agreement between the previous and the present experimental data, and also between both experimental data sets and the BSR and CCC

Differential cross sections for $n = 2$ states of helium at intermediate energies (80 eV, 100 eV and 120 eV) measured across the complete angular scattering range (0°-180°).

predictions across the angular range. RMPS deviates slightly from these results at large angles above 150°, similarly to the behaviour at the lower energy of 80 eV discussed above. The FOMBT model overestimates the cross section beyond 100°, and both the 5-state BSR and the FOMBT results deviate from the other data sets in the range 15° - 60°. There is also a minor difference in the experimental and theoretical data sets below 5°.

The 2^1S DCS shows very good agreement with the theoretical data, apart from the 5-state predictions that suggest a higher cross section across the entire angular range. This is a typical problem in models with insufficient channel coupling accounted for. The shape and magnitude of the DCS are in agreement across almost all of the angular range even within the small uncertainties of the experimental values. The only regions with slight but noticeable discrepancies are between 110º and 150º, where the experimental results suggest a slight dip, and below 5°. Generally even at very large and very small angles the agreement is excellent. The agreement is slightly better with the CCC results, but both BSR and RMPS agree well up to 120° before there is slight divergence both between the models and with the experimental and CCC data, both of which suggest a slightly smaller cross section.

The measured 2^3P DCS error bars are relatively larger beyond 90°. This means there are limited conclusions that can be drawn from this comparison. However, the current experimental results agree broadly with the theoretical data above 25º. Beyond 120º the experimental data have larger uncertainties because of the low counting rates for the 2^3P state in this angular range. Looking at the overall trend, however, the theoretical values tend to lie slightly above the experimental data and are in general agreement with each other, again with the exception of the 5-state numbers. Below about 25º the experimental data again deviate strongly from the theoretical predictions, with the latter showing a local maximum near 25º and decreasing from 25º down to 0º. The present experimental data, on the other hand, increase from 25º towards 0º. Again the discrepancy could be due to a contribution to the measured signal from the neighbouring 2^1P state, which has been modelled by adding a 1% 2^1P contribution to the RMPS model. These results also support the previous experimental data of Trajmar et al [1].

The measured 2^3S DCS again shows the least agreement with the theoretical predictions. The experimental data of both the current and previous work suggest that the cross sections from the theoretical models may be slightly high. For all data, with the exception of the 5-state results, the theoretical angular dependence is similar to the experimentally determined shape, but the absolute data lie above the experimental data points over most of the angular range. The dip near 30º and a suggested dip between 80° and 90° appear in both the theoretical and experimental data. The differences at small angles (less than 30°) at all three energies require further investigation elsewhere, but possible causes are discussed briefly here. As the energy increases from 80 eV to 120 eV, the shape of the theoretical and experimental data tends to become flatter over the angular range 30° to 180°

and the steepness shallows for the region 0° to 30°. Whilst the current experimental data follows this general trend, the DCS near 0° dips at 100 eV before increasing again at 120 eV, The increase at 120 eV is a cause for concern as the expectation would be for this to decrease. This may be as a result of a small geometrical distortion in the normalisation technique giving a slight difference in line shape at very small angles (below 10°), though there is no clear reason why this should be the case. It may also be due to changes in the overlap of gas and electron beams as the energy increases. The experimental data of Trajmar et al suggests that the current experimental data overestimates the DCS from 0° to 10°, and underestimates the DCS from 10° to 30°. Work on the out-of-plane characteristics of the MAC will be published later, and further modelling of the overlap in the current data will be investigated as part of this work.

4.3 DCS results at 120 eV

Measurements of the DCS at 120 eV for the 2^3S, 2^1S, 2^3P and 2^1P states of helium are shown in figures 12 - 15. As before, the experimental results are presented together with theoretical predictions from the CCC, RMPS, and two BSR calculations. No further theoretical or experimental results are presented at this energy.

The 2^1P data show excellent agreement between the current experimental data and the theoretical models across the angular range. The 5-state numbers deviate slightly from these results between 15° and 30° and at large angles above 140°, again similar to the lower energy behaviour discussed above. There is also a minor difference between the experimental data and the BSR and RMPS theoretical results below 5°.

The 2^1S DCS again shows good agreement with the theoretical results, especially those from the BSR and CCC calculations, above 40°, with the exception of the 5-state results that are higher above 5°. The overall shape and magnitude of the experimental and theoretical DCS are in excellent agreement across almost the entire angular range. Even at very large and very small angles the agreement is good, although there are slight differences in the range between 10º and 30º, where the theoretical values lie above the experimental data. The RMPS cross section tends to be slightly higher up to 150°.

Again the measured 2^3P DCS error bars are relatively larger beyond 80°. However the current experimental results agree broadly with the predictions above 35º. Given the larger uncertainties in the experimental data the overall trend of the theoretical values tend to lie slightly above the experimental data, but at this energy there are fluctuations between both the models themselves, and between the models and the experimental data. The 5-state model again yields generally higher cross section than the other models at a given scattering angle. Below about 25º the experimental data again deviate strongly from the theoretical predictions, with the theoretical curves exhibiting a local maximum near 25º and decreasing from 25º down to 0º. The current experimental data, on the other hand, again increase from 25º towards 0º. As before, the discrepancy could be due to a contribution to the measured signal from the

neighbouring 2^1P state. Modelling this effect by adding a 1% 2^1P contribution to the RMPS results for the 2^1P state suggests that this may indeed be the case.

Not surprisingly, the 2^3S DCS shows the least agreement with the theoretical results at this energy as well. The experimental data of the current work again suggest that the cross sections predicted by the theoretical models may be slightly too high or that the experimental data is under-detecting the DCS based on the discussion on 2^3S at 100 eV. For all data, with the exception of the 5-state results, the theoretical shape of the curve is similar to the experimental shape, but the theoretical numbers lie above the experimental data points over most of the angular range. There appear to be dips near 30º and between 80° and 100° in both the theoretical and experimental results. Below 10º the theoretical values again tend to underestimate the DCS, the peak near zero is suggested to be experimentally erroneous as commented on for 2^3S at 100 eV. Above 130° there is some divergence between the experimental and theoretical results and amongst the theoretical predictions themselves. The BSR results are surprisingly different from those of the other models and the experimental data. The angular dependence is arguably most similar to the experimental data albeit with higher cross section values.

5. CONCLUSIONS

We have presented experimental data and calculated results of DCS for the 2^3S, 2^1S, 2^3P, and 2^1P states of helium for electrons with incident energies of 80, 100, and 120 eV. In general, there is quite good agreement between the experimental DCS and the theoretical predictions with respect to both the magnitude and the overall angular dependence of the cross sections, and good agreement with previous experimental data. Moreover, the level of agreement is similar for all the incident energies investigated. The agreement for the 2^1S state is particularly good. Where differences do occur, they are found mainly at large angles (above 150°) and small angles (below 30°) in the triplet states 2^3S and 2^3P. At small angles these differences in the 2^3P state are likely the result of limited experimental resolution. The remaining differences, however, particularly for the 2^3S near the forward direction, require further investigation. These conclusions support similar findings by Lange et al [7] at lower energies. The comparison of multiple theories with experiment at extreme angles provides a rigorous method of investigating these remaining differences, and the successful use of the magnetic angle changer at intermediate energies significantly broadens opportunities for comparing theory with experiment across the entire angular range.

Acknowledgments

The work of RW, DC, NB, GCK and FHR was supported by EPSRC grant GR/K90845/01, the work of DVF and IB was supported by the Australian Research Council, the Australian National Computing Infrastructure Facility and its Western Australian node Ivec, and the

Differential cross sections for $n = 2$ states of helium at intermediate energies (80 eV, 100 eV and 120 eV) measured across the complete angular scattering range (0°-180°).

work of OZ and KB was supported by the United States National Science Foundation under grants PHY-0757755 and PHY-0903818.

Differential cross sections for n = 2 states of helium at intermediate energies (80 eV, 100 eV and 120 eV) measured across the complete angular scattering range (0°-180°).

5 Figures

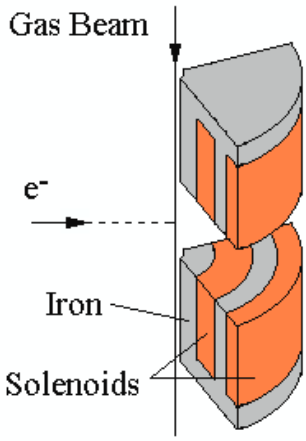

Figure 1 - A quarter cross section of the present iron-cored coil system. The total radius of the coil is 15 mm and the length of one coil is approximately 12 mm. The positions of the iron cores are shown at the top of the diagram by grey rectangles.

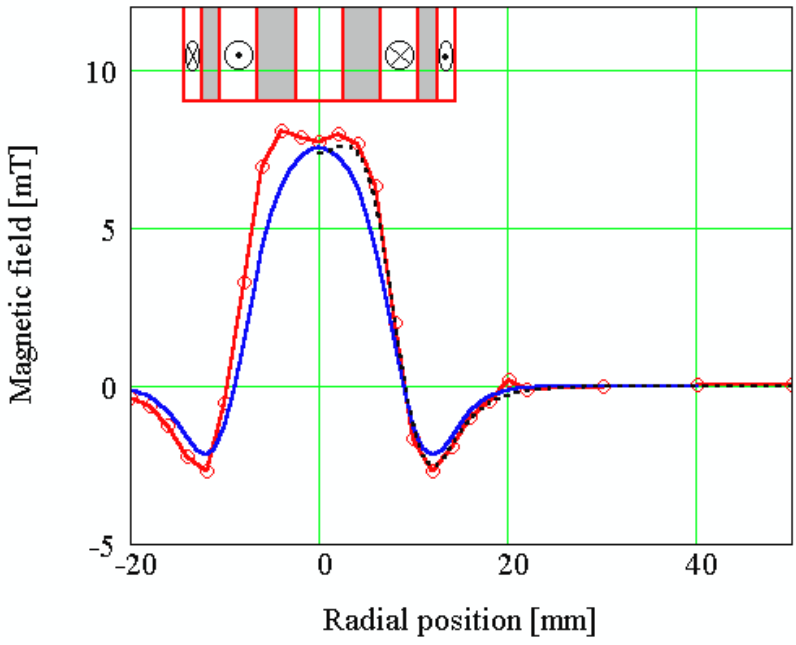

Figure 2 - The circles indicate magnetic field measurements for the complete coil system. The dotted line represents the calculated fields for the coil using Equation 1.The smooth curve without circles represents the magnetic field variation for a MAC without an iron core, scaled up by a factor of 5.

Differential cross sections for $n = 2$ states of helium at intermediate energies (80 eV, 100 eV and 120 eV) measured across the complete angular scattering range (0°-180°).

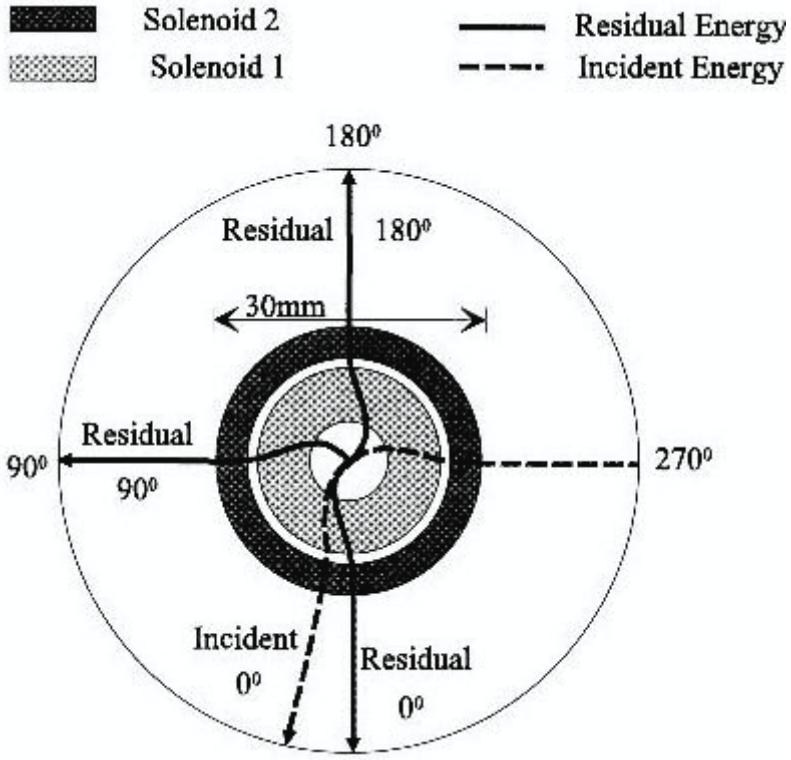

Figure 3 –Motion of electrons under the influence of the MAC for nominal incident and residual energies of 40 eV and 20 eV respectively. The incident beam enters the MAC from the right side of the figure. The effect of the applied currents within the MAC results in the straight-through beam (indicated by the dashed line) exiting the MAC at the bottom of the figure. This is separated from electrons scattered at 0° with lower residual energy (shown by the solid line) which also exit the MAC at the bottom of the figure, but experience a slightly stronger deflection. Electrons scattered at 90° and 180° (solid line to left of the figure and vertically upwards respectively) can also be detected by either moving the analyser, or by fixing the analyser and applying different currents to the MAC.

Differential cross sections for n = 2 states of helium at intermediate energies (80 eV, 100 eV and 120 eV) measured across the complete angular scattering range (0°-180°).

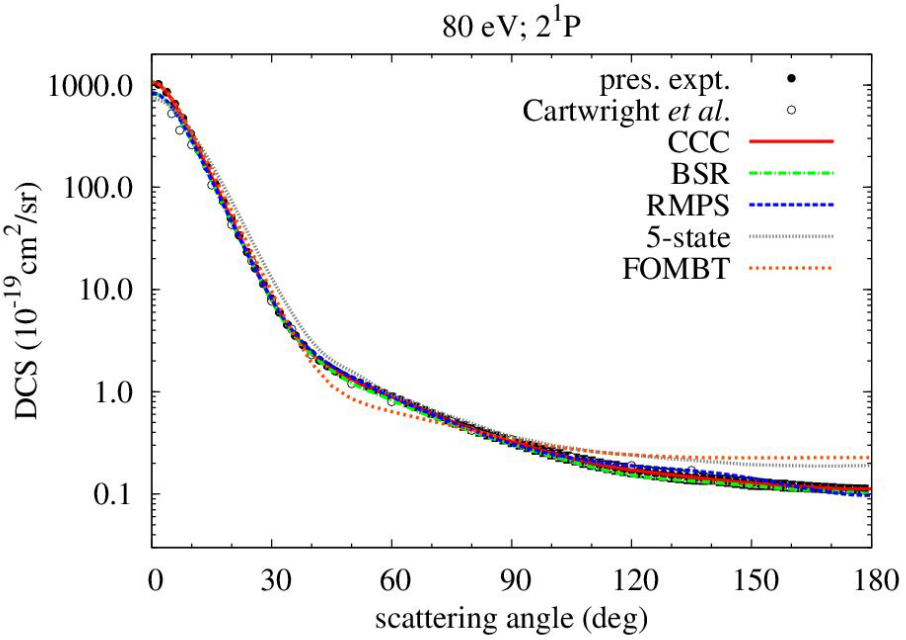

Figure 4 – DCS in Helium for the 2^1P state at 80 eV.

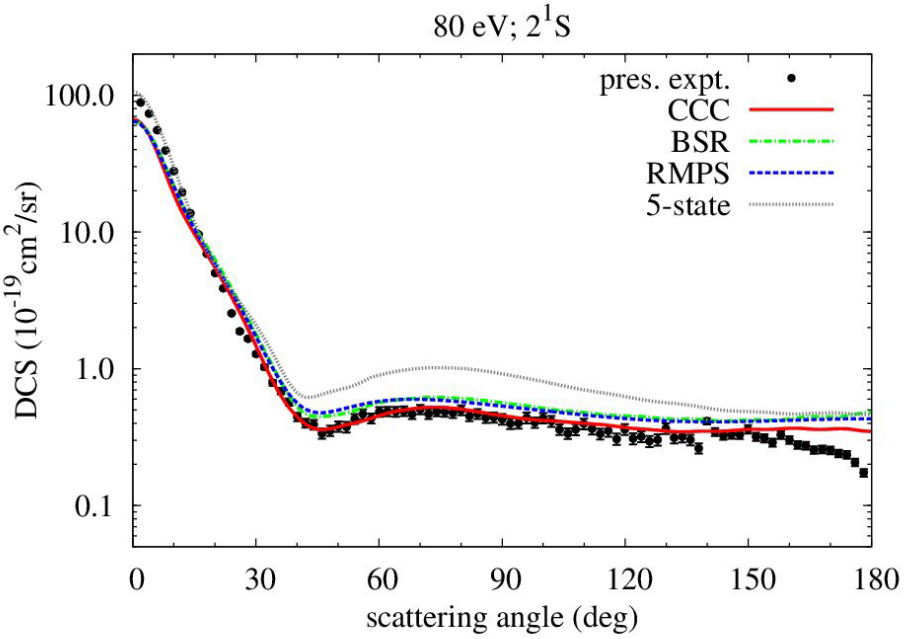

Figure 5 – DCS in Helium for the 2^1S state at 80 eV.

Differential cross sections for n = 2 states of helium at intermediate energies (80 eV, 100 eV and 120 eV) measured across the complete angular scattering range (0°-180°).

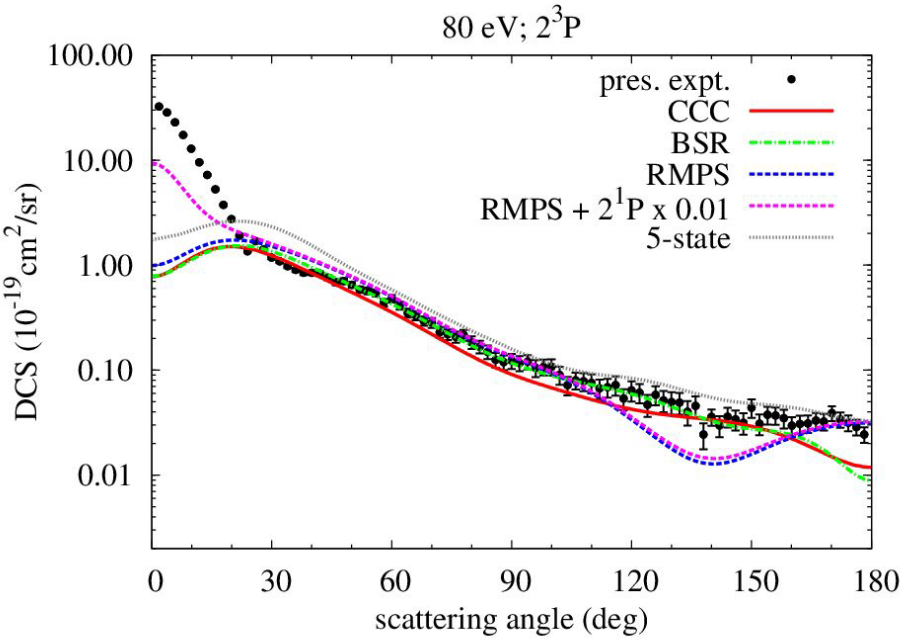

Figure 6 – DCS in Helium for the 2^3P state at 80 eV.

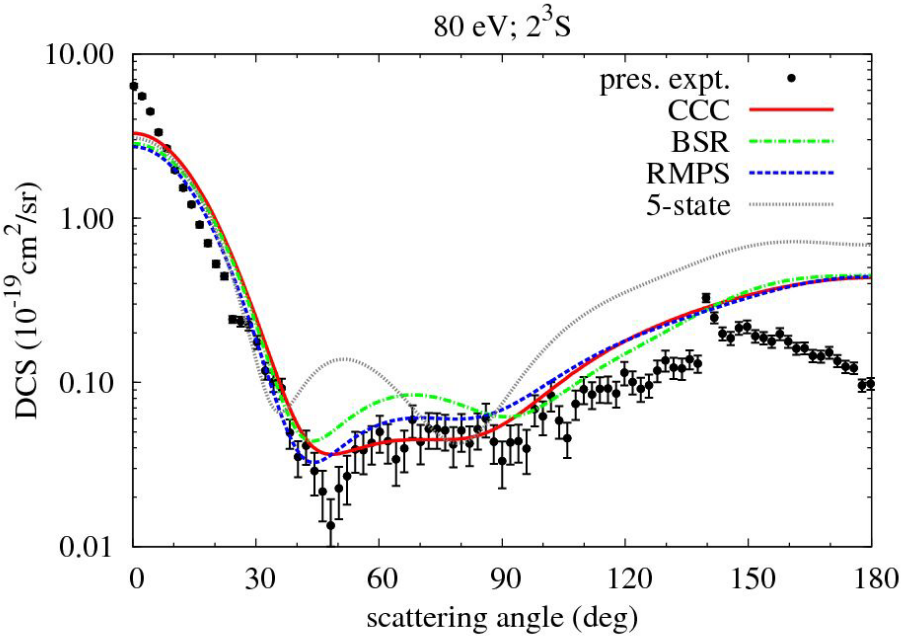

Figure 7 – DCS in Helium for the 2^3S state at 80 eV.

Differential cross sections for $n = 2$ states of helium at intermediate energies (80 eV, 100 eV and 120 eV) measured across the complete angular scattering range (0°-180°).

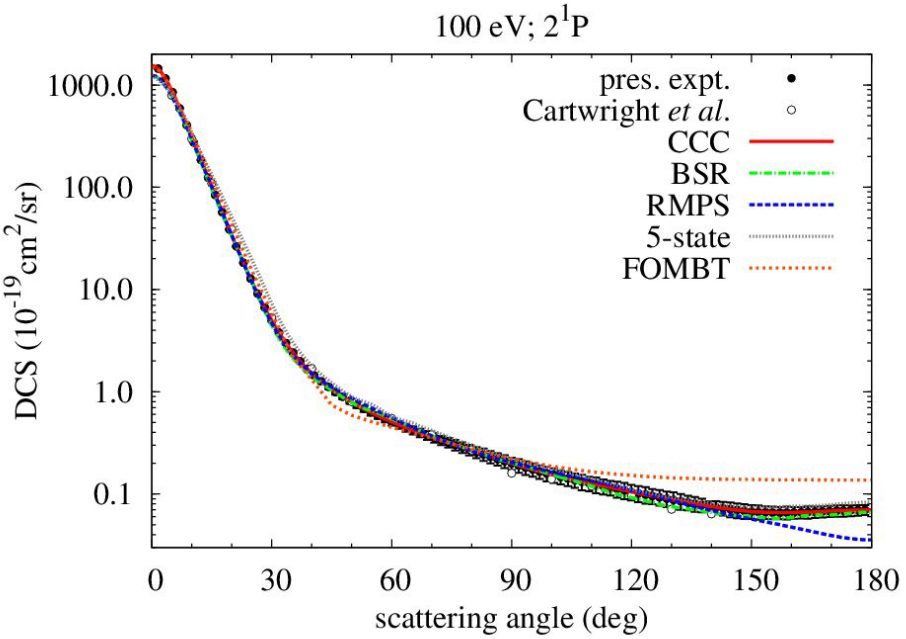

Figure 8 – DCS in Helium for the 2^1P state at 100 eV.

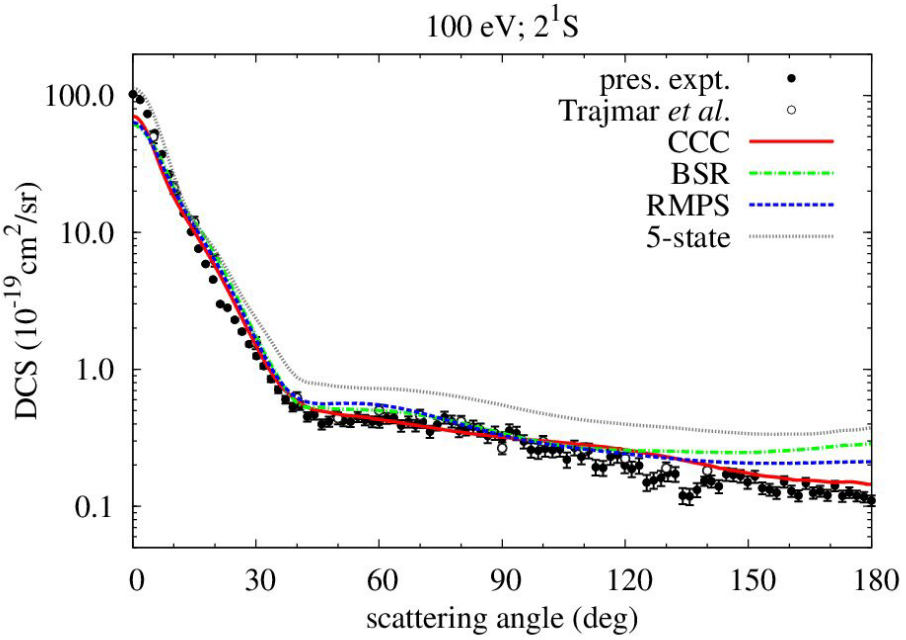

Figure 9 – DCS in Helium for the 2^1S state at 100 eV.

Differential cross sections for n = 2 states of helium at intermediate energies (80 eV, 100 eV and 120 eV) measured across the complete angular scattering range (0°-180°).

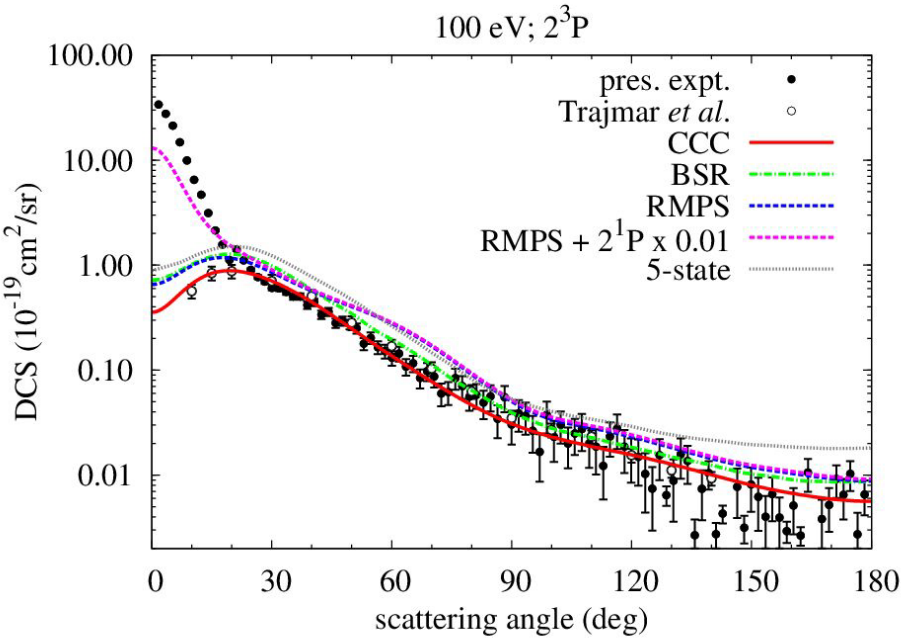

Figure 10 – DCS in Helium for the 2^3P state at 100 eV.

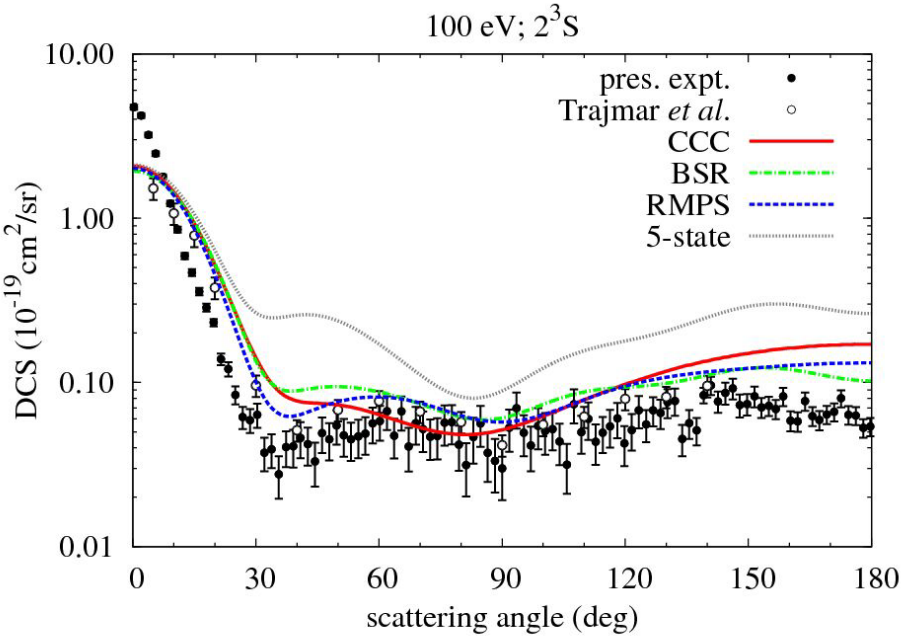

Figure 11 – DCS in Helium for the 2^3S state at 100 eV.

Differential cross sections for n = 2 states of helium at intermediate energies (80 eV, 100 eV and 120 eV) measured across the complete angular scattering range (0°-180°).

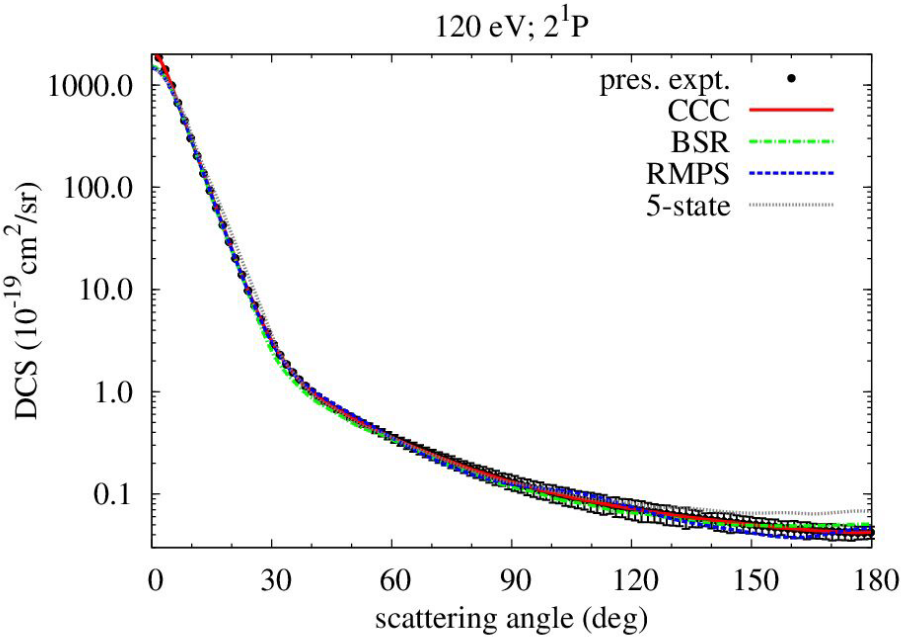

Figure 12 – DCS in Helium for the 2^1P state at 120 eV.

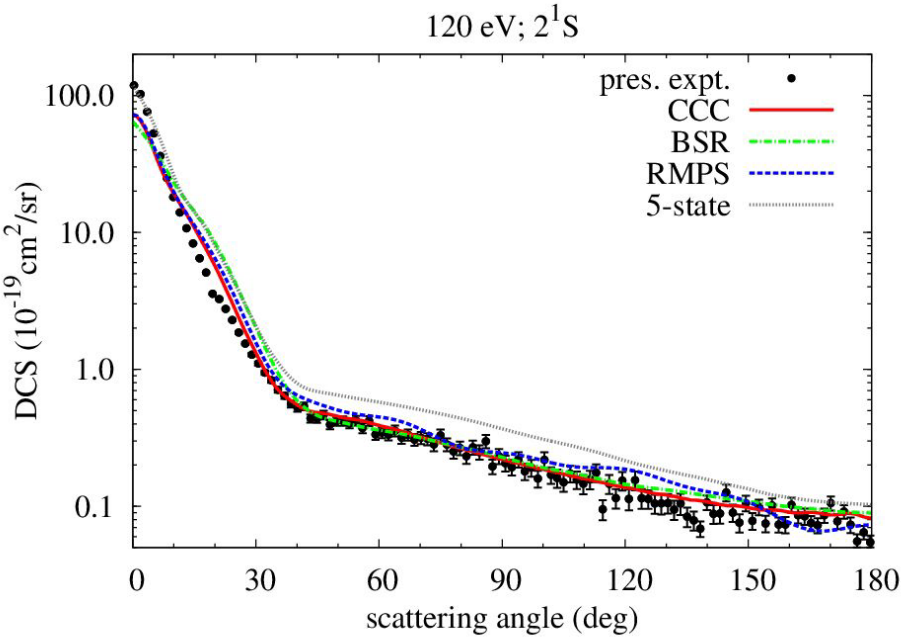

Figure 13 – DCS in Helium for the 2^1S state at 120 eV.

Differential cross sections for n = 2 states of helium at intermediate energies (80 eV, 100 eV and 120 eV) measured across the complete angular scattering range (0°-180°).

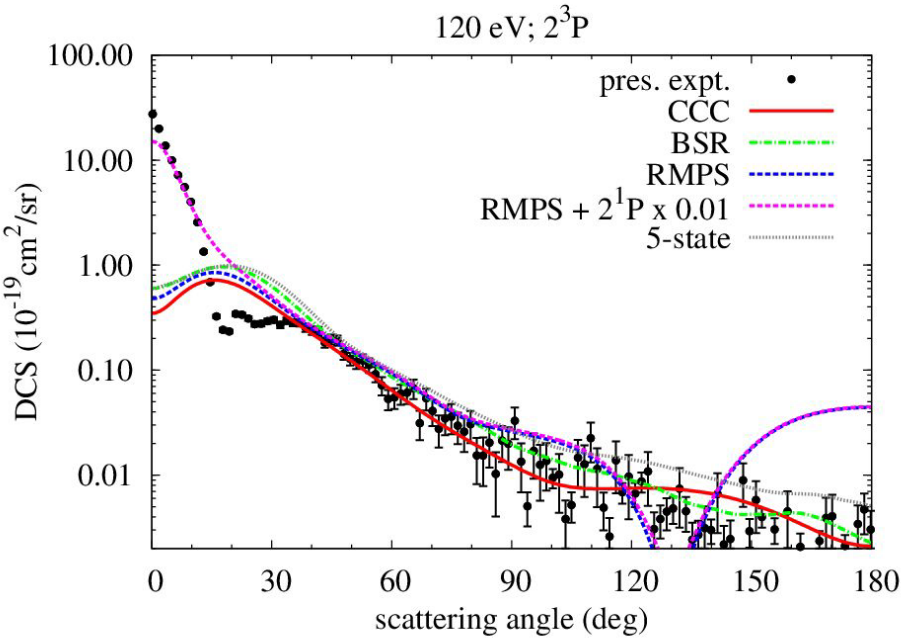

Figure 14 – DCS in Helium for the 2^3P state at 120 eV.

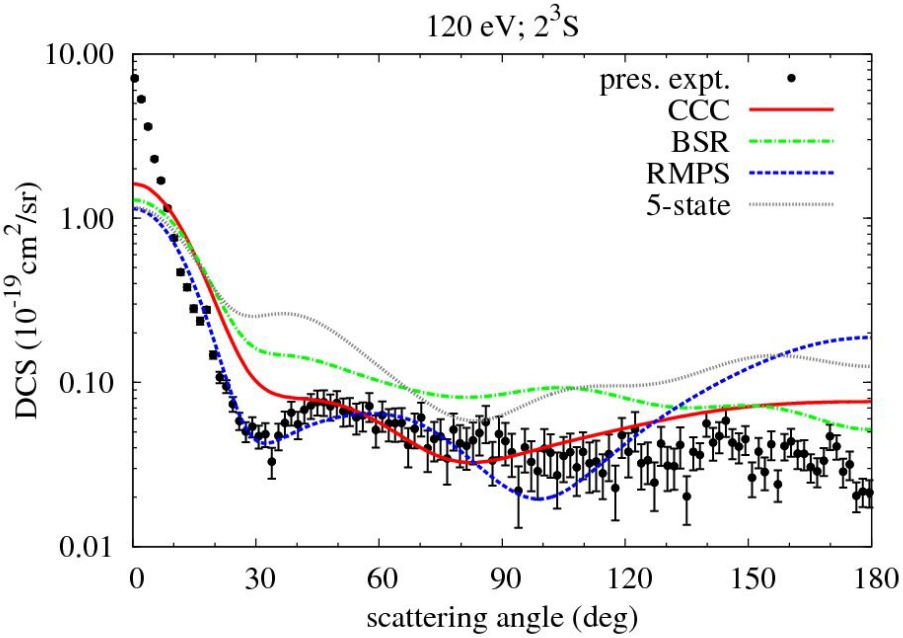

Figure 15 – DCS in Helium for the 2^3S state at 120 eV.

Differential cross sections for $n = 2$ states of helium at intermediate energies (80 eV, 100 eV and 120 eV) measured across the complete angular scattering range (0°-180°).

REFERENCES

[1] Trajmar S, Register D F, Cartwright D C and Csanak G 1992 *J. Phys. B: At. Mol. Opt. Phys.* **25** 4889-4910
[2] Allan M 1992 *J Phys B: At. Mol. Opt. Phys.* **25** 1559
[3] Röder J, Ehrhardt H, Bray I, Fursa D V and McCarthy I E 1996 *J Phys B: At. Mol. Opt. Phys.*, **29**, 2103
[4] Asmis K R and Allan M 1997 *J Phys B: At. Mol. Opt. Phys.*, **30,** 1961
[5] Cubric D, Mercer D J L, Channing J M, King G C and Read F H 1999 *J Phys B: At. Mol. Opt. Phys.* **32**, L45-50
[6] Allan M 2000 *J Phys B: At. Mol. Opt. Phys.* **33**, L215-20
[7] Lange M, Matsumoto J, Lower J, Buckman S, Zatsarinny O, Bartschat K, Bray I and Fursa D 2006 *J. Phys. B : At. Mol. Opt. Phys.*, **39**, 4179-4190
[8] Hoshino M, Kato H, Tanaka H, Bray I, Fursa D V, Buckman S J, Ingólfsson O and Brunger M J 2009 *J Phys B: At. Mol. Opt. Phys.* **42**, 145-202
[9] Hidalgo M D and Geltman S 1972 *J. Phys. B : At. Mol. Opt. Phys.*, **5**, 617
[10] Chutjian A and Srivastava S K 1975 *J. Phys. B : At. Mol. Opt. Phys.*, **8**, 2360-8
[11] Bartschat K and Madison D 1988 *J. Phys. B: At. Mol. Opt. Phys.*, **21**, 153-170
[12] Scott T and McDowell M R C 1975 *J. Phys. B : At. Mol. Opt. Phys.*, **8**, 2369
[13] Mansky E J and Flannery M K 1990 *J. Phys. B : At. Mol. Opt. Phys.*, **23**, 4573
[14] Bransden B H and Winters K H 1975 *J. Phys. B: At. Mol. Opt. Phys.*, **8**, 1236-44
[15] Bartschat K, Hudson E T, Scott M P, Burke P G and Burke V M 1996 *J. Phys. B: At. Mol. Opt. Phys.*, **29**, 115-123
[16] Zatsarinny O 2006 Comp. Phys. Commun. 174, 273.
[17] Fursa D V and Bray I 1997 *J. Phys. B : At. Mol. Opt. Phys.*, **30**, 757-85
[18] Read F H and Channing J M 1996 *Rev. Sci. Instrum.*, **67**, 2373
[19] Zubek M, Gulley N, King G C and Read F H 1996 *J. Phys. B: At. Mol. Opt. Phys.*, **29**, L239
[20] Bradford R C 1978 Ph.D. Thesis, Victoria University of Manchester
[21] Channing J M 1998 Ph.D. Thesis, Victoria University of Manchester
[22] Gopalan A, Bömmels J, Götte S, Landwehr A, Franz K, Ruf M W, Hotop H, and Bartschat K 2003 *Eur. Phys J D*, **22,** 17
[23] Mercer D 1997 Ph.D. Thesis, Victoria University of Manchester
[24] Trajmar S and Register D F 1984 *Electron-Molecule Collisions* ed. I Shimamura and K Takayanagi (New York: Plenum) Chapter 6, pp 427-93
[25] Chamberlain G E, Mielczarek S R and Kuyatt C E 1970 *Phys. Rev. A,* **2**, 5, 1905-23
[26] Srivastava S K, Chutjian A and Trajmar S 1975 *J. Chem. Phys.*, **63**, 2659-65
[27] Joyez G, Huetz A, Pichou F and Mazeau J 1976 *Electron and Photon Interactions with Atoms* (New York: Plenum) New measurements of differential and integral cross sections for electron excitation of the n=2 states of helium pp 349-64
[28] Bartschat K, Hudson E T, Scott M P, Burke P G and Burke V M 1996 *J. Phys. B: At. Mol. Opt. Phys.*, **29**, 115-23
[29] Bartschat K 1998 *Comp. Phys. Commun.* **114** 168
[30] Bartschat K, Hudson E T, Scott M P, Burke P G and Burke V M 1996, *Phys. Rev. A* **54** R998
[31] Zatsarinny O and Fischer C F 2000 *J. Phys. B: At. Mol. Opt. Phys.*, **33**, 313-41
[32] Zatsarinny O and Bartschat K 2004 *J. Phys. B: At. Mol. Opt. Phys.* **37** 2173
[33] Burke P G and Berrington K A 1993 *Atomic and Molecular Processes: an R-Matrix Approach* (Institute of Physics Publishing, Bristol)
[34] Berrington K A, Eissner W B and Norrington P N 1995 *Comp. Phys. Commun.* **92** 290
[35] Csanak G, Taylor H S and Yaris R 1971 *Phys. Rev. A,* **3** 4 1322-8
[36] Cartwright D C, Csanak G, Trajmar S and Register D F 1992 *Phys. Rev. A,* **45** 1602-24
[37] Opal C B and Beaty E C 1972 *J. Phys. B: At. Mol. Opt. Phys.*, **5**, 627-35